Nanoscale Advances

ROYAL SOCIETY OF CHEMISTRY

PAPER

View Article Online
View Journal | View Issue

Cite this: *Nanoscale Adv.*, 2025, **7**, 2255

Engineering a multivariate cobalt metal–organic framework for high photocatalytic activity: the impact of mixed ligands and metal incorporation in a visible light-driven heterogeneous photo-Fenton reaction for water treatment†

Noelia Rodríguez-Sánchez, [ab] Biswajit Bhattacharya, [a] Franziska Emmerling, [ac] Carsten Prinz, [a] Paula Prieto-Laria, [d] A. Rabdel Ruiz-Salvador *[ae] and Menta Ballesteros *[bd]

Metal–organic frameworks (MOFs) have attracted increasing attention for the removal of organic pollutants in wastewater *via* photocatalysis. Here, we design a multivariate modification of ZIF-9 to tune its electronic properties for use in visible light photocatalysis. A controllable synthesis of ZIF-9 and its multivariate forms with the incorporation of copper and the 2-imidazolecarboxaldehyde (ica) ligand was carried out. The materials are tested for the removal of the model dye methylene blue (MB) by a heterogeneous photo-Fenton-like reaction at neutral pH and room temperature. Cu-ZIF-9-ica (UPO-3) shows high photocatalytic activity under both visible and ultraviolet A (UVA) light, achieving 94% MB degradation in 45 min, compared to 65% MB degradation in 120 min using bare ZIF-9. The study revealed a first-order rate constant of 0.0475 min^{-1} for Cu-ZIF-9-ica compared to 0.0088 min^{-1} for ZIF-9 under visible light. The improvement of the catalyst was clearly attributed to the co-incorporation of Cu and the ica ligand in the MOF, which reduces the band gap, in agreement with DFT calculations. Reproducibility and recyclability tests proved that Cu-ZIF-9-ica can be used for at least 3 cycles without a significant loss of efficiency, making it a promising material for the study and application of wastewater treatment.

Received 18th November 2024
Accepted 5th February 2025

DOI: 10.1039/d4na00954a

rsc.li/nanoscale-advances

Introduction

Materials design at the nanoscale plays a crucial role in addressing global problems. Nowadays, water scarcity is one of the most pressing global challenges exacerbated by population growth and climate change. Increasing demand for freshwater in agriculture, industry, and domestic use strains traditional sources.[1] Water reuse is a viable strategy to address this challenge, promoting circular economy principles by closing the loop on water usage, thereby reducing reliance on external water supplies and mitigating environmental impacts associated with excessive water extraction.[2] Effective water reuse requires the removal of pollutants from wastewater, especially emerging contaminants that affect human health and ecosystems. The inadequacy of current pollutant removal systems has led researchers to explore Advanced Oxidation Processes (AOPs) for more effective elimination of these toxic compounds.[3–6]

AOPs are highly effective in removing a wide range of contaminants. Among them, Fenton-based processes produce non-selective hydroxyl radicals (˙OH) from a metal that is easy to oxidize/reduce, commonly iron, and H_2O_2.[7] The efficiency improves with radiation, such as solar or UV light, in a process known as photo-Fenton. In a typical heterogeneous photo-Fenton process, metal ions immobilized on a solid support react with H_2O_2 under UV/visible light, creating electron–hole pairs and ˙OH radicals, which decompose contaminants.[8] In recent decades, MOFs have been extensively studied for their use as solid supports in these processes due to their exceptional properties.[8] These materials, consisting of metal ions or metal-containing clusters linked by organic ligands, form versatile structures.[9] Their high surface area, multiple active sites, and ability to easily extract as solid catalysts and use at near-neutral pH make them more efficient than traditional catalysts.[10] Additionally, MOFs can be engineered with specific electronic

[a]*BAM Federal Institute for Materials Research and Testing, Richard-Willstätter-Straße 11, 12489, Berlin, Gemany*

[b]*Center for Nanoscience and Sustainable Technologies (CNATS), Universidad Pablo de Olavide, Ctra. Utrera Km. 1, 41013, Seville, Spain. E-mail: mmbalmar@upo.es*

[c]*3Department of Chemistry, Humboldt-Universität of Berlin, Brook-Taylor-Strasse 2, 12489 Berlin, Germany*

[d]*Department of Molecular Biology and Biochemistry Engineering, Universidad Pablo de Olavide, Ctra. Utrera Km. 1, 41013, Seville, Spain*

[e]*Department of Physical, Chemical and Natural Systems, Universidad Pablo de Olavide, Ctra. Utrera Km. 1, 41013, Seville, Spain. E-mail: rruisal@upo.es*

† Electronic supplementary information (ESI) available. See DOI: https://doi.org/10.1039/d4na00954a

properties and reduced band-gaps to improve solar energy absorption and $^{\bullet}OH$ production.[8,11] While metal doping is known to improve photocatalytic efficiency, the impact of mixed ligands has been less addressed.[12] Recent studies have shown that by mixing both metals and ligands results in multivariate MOFs with enhanced catalytic activity.[13,14]

Among MOFs, ZIF-9, composed of cobalt ions linked to a benzimidazole ligand (bml), belongs to zeolitic imidazolate frameworks (ZIFs), a subclass of MOFs consisting of tetrahedral metal atoms linked by imidazolate groups.[15] This ZIF has been used in various photocatalytic reactions like hydrogen generation and oxidation reactions,[16] where it has been typically used as a support for other photocatalytic materials rather than as a standalone photocatalyst. Theoretical studies have shown that mixing ligands or metals in ZIFs can modify the electronic structure to absorb light in the visible range of the electromagnetic spectrum.[17] Such a molecular engineering approach could be used to enhance the light absorption properties of ZIF-9 and unleash its full photocatalytic potential. Therefore, the aim of this study is to enhance the photocatalytic activity of ZIF-9 for the degradation of organic compounds in water. To this purpose, a conceptual design is used for engineering the electronic properties of ZIF-9 by modifying the structure through the incorporation of copper or 2-imidazolecarboxaldehyde (ica) to form multivariate MOFs, considering that both copper and ica can have a significant effect on the electronic structure of ZIFs. The photocatalytic efficiency of these compounds was tested in a heterogeneous photo-Fenton-like reaction under visible and UVA light for model dye methylene blue (MB) degradation. Additionally, the stability and recyclability of the material with better properties were verified. The reaction was carried out at neutral pH and ambient temperature to evaluate its potential for degrading water contaminants and promoting water reuse.

Materials and methods

Synthesis and characterization of the materials

Details of the reagents used for the synthesis of ZIF-9, Cu-ZIF-9 and Cu-ZIF-9-ica can be found in the ESI.† ZIF-9 was synthesized by a typical solvothermal method, following the report by He *et al.*[18] with some minor modifications. A solution of 1 mM bml (0.120 g) in 8.68 mL of EtOH was prepared and stirred for 5 min. Then, 0.21 mL ammonia hydroxide was added to the solution and stirred with a magnetic stirrer for 10 min. Subsequently, 0.5 mM $Co(NO_3)_2\cdot 4H_2O$ (0.125 g) was added to the beaker and stirred for 3 h at room temperature (25 °C). After 3 h, the samples were washed and centrifuged with ethanol 3 times and allowed to dry in an oven for 12 h (80 °C).

For Cu-ZIF-9 synthesis, 0.120 g of bml was dissolved in a beaker (A) with 5 mL of ethanol and stirred for 5 min. Concurrently, 0.118 g of $Co(NO_3)_2\cdot 6H_2O$ and 6 mg of $Cu(CO_2CH_3)_2\cdot H_2O$ were dissolved in 3.7 mL of EtOH in a beaker (B) and stirred for 10 min. Then, 0.21 mL of ammonia hydroxide was added to the beaker (A) and, after 10 min, solution B was added to the beaker (A). After 3 h at room temperature (25 °C), the samples were washed and centrifuged with EtOH 3 times and allowed to dry in an oven for 12 h (80 °C). The procedure for the synthesis of Cu-ZIF-9-ica was the same, but with a slight modification in the initial quantity of the beaker (A), in which 0.117 g of bml and 2 mg of ica were dissolved in 8.67 mL of EtOH. The following steps were the same as those of Cu-ZIF-9.

The molar ratio used for the synthesis of ZIF-9 was 0.5 : 1 : 148 for the reagents $Co(NO_3)_2\cdot 4H_2O$: bIm : EtOH. For Cu-ZIF-9, it was 0.47 : 0.03 : 1 : 148 for the reagents $Co(NO_3)_2\cdot 4H_2O$: $Cu(CO_2CH_3)_2\cdot H_2O$: bIm : EtOH, and for Cu-ZIF-9-ica, it was 0.47 : 0.03 : 0.98 : 0.02 : 148 for the reactants $Co(NO_3)_2\cdot 4H_2O$: $Cu(CO_2CH_3)_2\cdot H_2O$: bml : ica : EtOH.

The characterization details of the materials can be found in the ESI.† DFT calculations were performed with the CP2K code.[19] The band gaps were computed using the hybrid HSE06 functional,[20] which has been shown to be very effective in several materials including MOFs.[21] The REPEAT charges were computed,[22] as they are known to be a good descriptor in MOFs,[23] and thus can be useful to rationalize the role of the modifications. Further computational details are available in the ESI.†

Photo-Fenton experiments

Two 50 mL jacketed reactors were placed on a magnetic stirrer at 800 rpm. For visible light experiments, 1200 24 W lumen LED strips were affixed around one of the reactors (Fig. S.1†), while for the UVA test, the reactor was placed under a 14 W, 365 nm UVA lamp . The reactors were carefully covered with aluminium foil to prevent damage due to the UVA light and at the same time ensured the maximum incidence of light on the sample. To keep the temperature of the experiment constant (25 °C), the reactors were connected by cooling tubes to a thermostatic water bath.

To assess the photo-Fenton activity of the materials, a series of tests were conducted. A solution of 5 mg L^{-1} of MB and 0.5 g L^{-1} of the catalyst was added to the reactor, stirring at 800 rpm and at a temperature of 25 °C. The first 60 min were in the dark to evaluate the adsorption removal of MB by the catalysts. Subsequently, 35 μL of H_2O_2 were added to achieve an initial concentration of 10 mM in one of the reactors and the UVA light was turned on to conduct the photocatalytic test. The same procedure was performed with the other reactor using visible light. The experiments were studied for 120 min. From the beginning of the experiments, every 15 min, samples were taken, centrifuged, and the light absorbance of the supernatant was measured at 664 nm. The samples were returned to the reactor to avoid loss of the catalysts and solution volume. Also, to ensure the reproducibility of the work, several replications were carried out for each catalyst under each light condition. Moreover, control experiments were carried out under the same conditions as photo-Fenton assays to analyse the influence on MB removal by adsorption, photolysis, combined H_2O_2/UVA or visible light, and without the addition of H_2O_2.

In order to analyse the production of hydroxyl radicals of the reactions using Cu-ZIF-9-ica (UPO-3) as the catalyst and its parent material ZIF-9, *p*-nitrosodimethylaniline (RNO) was used

as a probe compound and spin trap for the detection of hydroxyl radicals.[24] This compound is highly selective for hydroxyl radicals and can be easily detectable using UV-vis spectroscopy. Tests were carried out under the same conditions as those used for photo-Fenton experiments. A solution of 17 μM of RNO and 0.5 g L^{-1} of the catalyst was added to a 50 mL reactor. 35 μL of H_2O_2 was added to achieve a solution of H_2O_2 10 mM. UVA or visible light was turned on for 120 min. The solution was stirred at 800 rpm, with an initial pH of 7 and a temperature of 25 °C. The samples were measured using a UV-vis spectrophotometer at 440 nm.

The Langmuir–Hinshelwood model[25] was used to explain the first-order kinetics (eqn (1)) of the photo-Fenton test:

$$\ln\frac{[C]}{[C]_0} = -k_r K t \quad (1)$$

where [C]: concentration in each point, [C_0]: initial concentration, k_r: limiting rate constant of the reaction at maximum coverage under the given experimental conditions, K: equilibrium constant for adsorption of the substrate onto the catalyst and t: time.

To verify the recyclability of UPO-3 (Cu-ZIF-9-ica), three consecutive decontamination tests were carried out with the same sample under UVA light and another three under visible light. After each cycle and once the decontamination tests were completed, the catalyst was recovered by centrifuging the final solution and washing it with ethanol. The latter causes the catalyst to precipitate due to weight gain by adsorption, facilitating its recovery. The samples were dried in an oven for 1 h at 50 °C. XRD measurements were carried out on Cu-ZIF-9-ica after 3 cycles of photo-Fenton tests to confirm the structural stability of the material after the photocatalytic process.

Results and discussion

Preparation and characterization of MOFs

A schematic representation of the synthesis of Cu-ZIF-ica (UPO-3) is presented in Fig. 1a. The synthesis of ZIF-9, Cu-ZIF-9, and Cu-ZIF-9-ica was successfully achieved and corroborated by XRD (Fig. 1b). The intensity and position of the peaks match the simulated PXRD pattern, built from the crystal structure reported by Park *et al.*[15] The results support the homogeneity of the samples and the absence of unwanted MOF phases, as well as the high crystallinity of these ZIFs. It is observed that doping copper and the copper-2-imidazolecarboxyaldehyde mixture does not result in a significant alteration in the structure. The results were also compared with the studies of He *et al.*,[18] corroborating that the substitution of dimethylformamide (DMF) for ethanol as a solvent for the synthesis of these MOFs is possible.

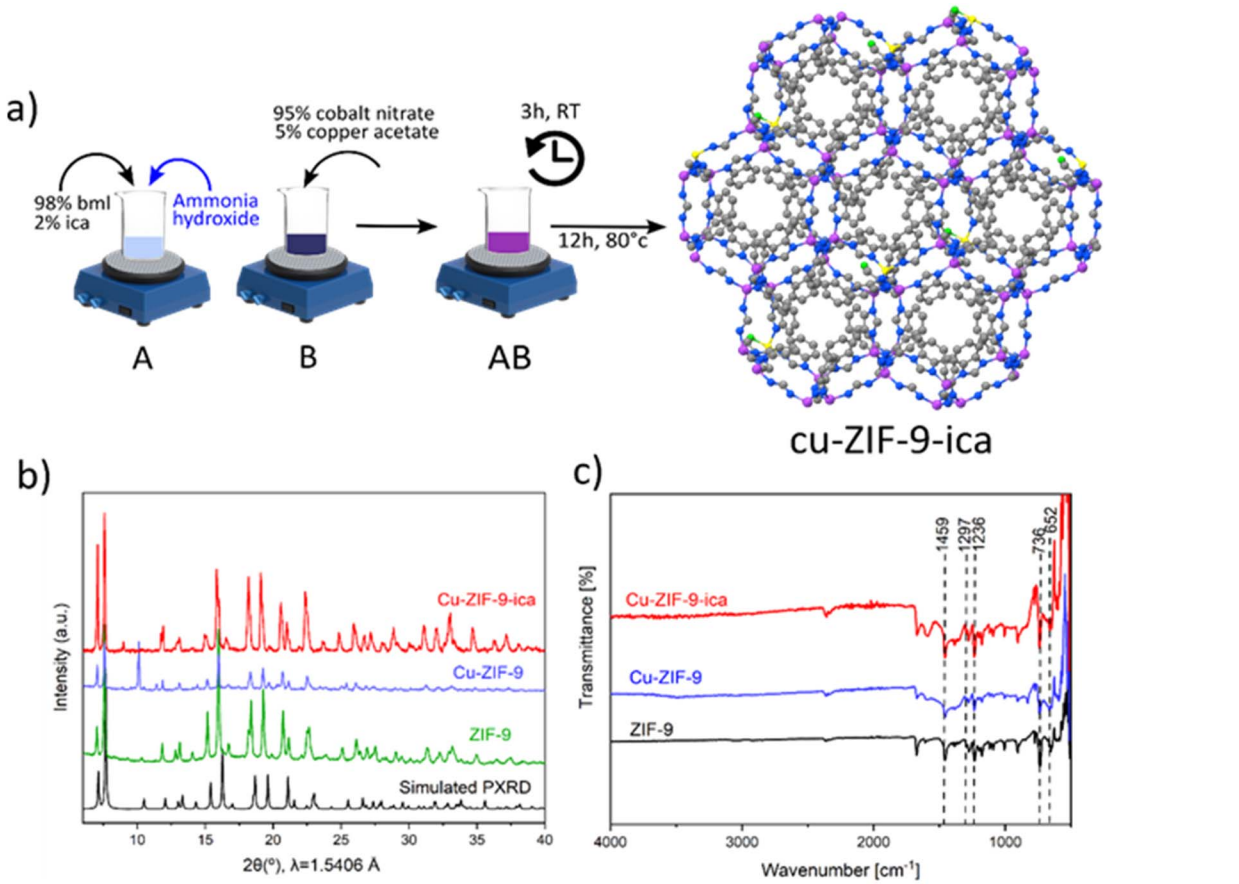

Fig. 1 Schematic representation of the synthesis method of Cu-ZIF-9-ica (a), X-ray diffraction data of simulated ZIF-9 (black), synthesized ZIF-9 (green), Cu-ZIF-9 (blue), and Cu-ZIF-9-ica (red) (b) and FT-IR spectra for ZIF-9 (black), Cu-ZIF-9 (blue) and Cu-ZIF-9-ica (red) (c).

The FT-IR spectroscopy results of ZIF-9 (Fig. 1c) agree with those of Öztürk *et al.*,[26] finding similarity in all the absorption bands. More intense bands were identified corresponding to C–C at 1236 cm^{-1}, C=C at 1459 cm^{-1}, C–N at 1297 cm^{-1}, and C–H at 736 cm^{-1} belonging to the benzimidazole ligand and C–C–C at 652 cm^{-1} corresponding to the characteristic peak of ZIF-9. A small band was identified in Cu-ZIF-9-ica at 1700 cm^{-1} (Fig. S.2†), which was attributed to the vibration of C=O bonds of the aldehyde group in 2-imidazolecarboxyaldehyde.[27]

While the incorporation of the ligand cannot be confirmed by the EDS technique due to the similarities with the composition of benzimidazole, the presence of Cu^{2+} ions in the structure of ZIF-9 could be confirmed in both Cu-ZIF-9 and Cu-ZIF-9-ica (Fig. S.3†). This suggests the presence of multiple active sites,[28] as well as the formation of CuO, as revealed by the increase in oxygen atoms in the samples.[29] SEM analysis revealed different morphology particles for each sample (Fig. 2). SEM images (Fig. 2a–c) reveal the overall morphology and size distribution of the particles, with sizes around 50 μm, in agreement with Park *et al.*[15] A cubic particle morphology was identified for ZIF-9, as was described in previous studies.[30] However, hexagonal particles grow in the case of multivariate Cu-ZIF-9-ica. This has been reported in previous work, where morphology control was found in mixed ligand ZIFs.[31] TEM images (Fig. 2d–f) reveal the nanoscale morphology of the incipient particles that had not yet reached the growth stage at the time of the synthesis. For the three materials, these nanoparticles show different shapes, with only ZIF-9 resembling microscale particles (Fig. 2a–c). This indicates that the formation of the multivariate ZIF would require more time to achieve the final morphology, as is typical in Ostwald ripening in ZIFs.[32] Note that the well facetted large particles (Fig. 2a–c), with clear edges, indicate that they are not agglomerates of smaller particles (approximately 100 times smaller).

In the Cu-ZIF-9 sample, Cu can be identified in wire-like or flake-like structures attributed to the formation of copper oxide layers on the surface of the MOF.[33] STEM analysis further confirms the uniform distribution of Cu in the samples (Fig. S.4†), finding 3.85% and 5.02% of the metal in Cu-ZIF-9 and Cu-ZIF-9-ica samples, respectively (Table S.1†). The absence of wire structures in the Cu-ZIF-9-ica sample, coupled with the uniformity of the morphology, suggests that Cu has been successfully incorporated into the framework of this material. The BET results revealed an increase in the specific surface area for Cu-ZIF-9-ica of 94.72 m^2 g^{-1} compared to that obtained for Cu-ZIF-9 (83.05 m^2 g^{-1}) and for ZIF-9 (75.38 m^2 g^{-1}) (Table S.2†). This decrease in the surface area of conventional ZIF-9 is in agreement with results published by other authors, who reported the synthesis of ZIF-9 and ZIF-7 using solvents other than DMF and under room temperature conditions.[34,35] However, the significant increase in the surface area of Cu-ZIF-9-ica indicates that the introduction of the aldehyde functional group in Cu-ZIF-9-ica has a positive effect in this regard as well. The high stability is also confirmed by TGA spectroscopy (Fig. S.5†), which showed structural stability up to 580 °C for all the samples. These results are in agreement with those published by other authors on ZIF-9.[15,26] These findings indicate that the incorporation of a metal, such as copper, or a mixed ligand, such

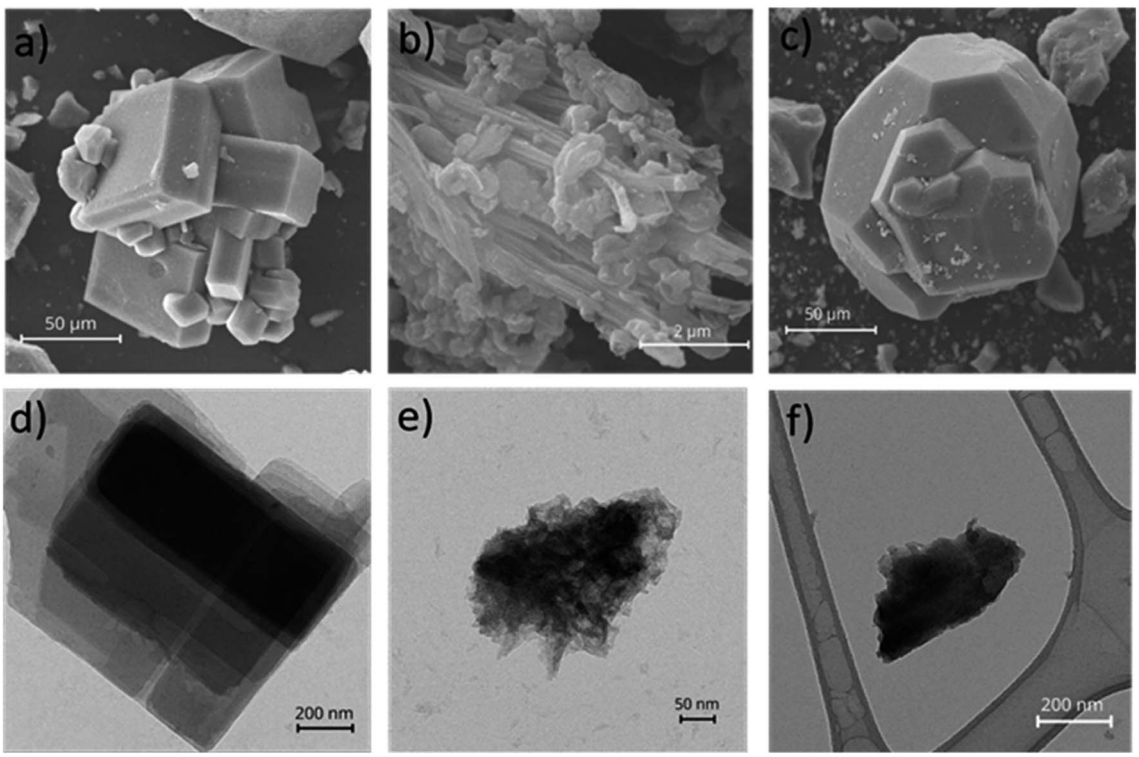

Fig. 2 SEM images of ZIF-9 (a), Cu-ZIF-9 (b) and Cu-ZIF-9-ica (c) with the respective scale bars of 50 μm, 2 μm and 50 μm. TEM images for ZIF-9 (d), Cu-ZIF-9 (e) and Cu-ZIF-9-ica (f) with the respective scale bars of 200 nm, 50 nm and 200 nm.

as 2-imidazolecarboxaldehyde, in small quantities does not affect the thermal stability of the material and enhances its applicability over a wide temperature range, rendering it a highly promising material for use in various applications.

Photo-Fenton experiments

The capacity of the materials to remove the dye was evaluated under different conditions. Before turning on the light, the concentration values were stable in adsorption experiments, with only 5% MB removal, which means that the adsorption is not a significant process in MB removal for these materials (Fig. 3a). Additionally, MB was photolyzed under visible and UVA radiation only for up to 20% in 120 min (Fig. 3b). This is attributed to the light absorption ability of the oxidized state of MB in the visible and UVA ranges of the electromagnetic spectrum, giving rise to photochemical reactions that begin from the singlet or triplet excited state (1D* and 3D*) of the dye

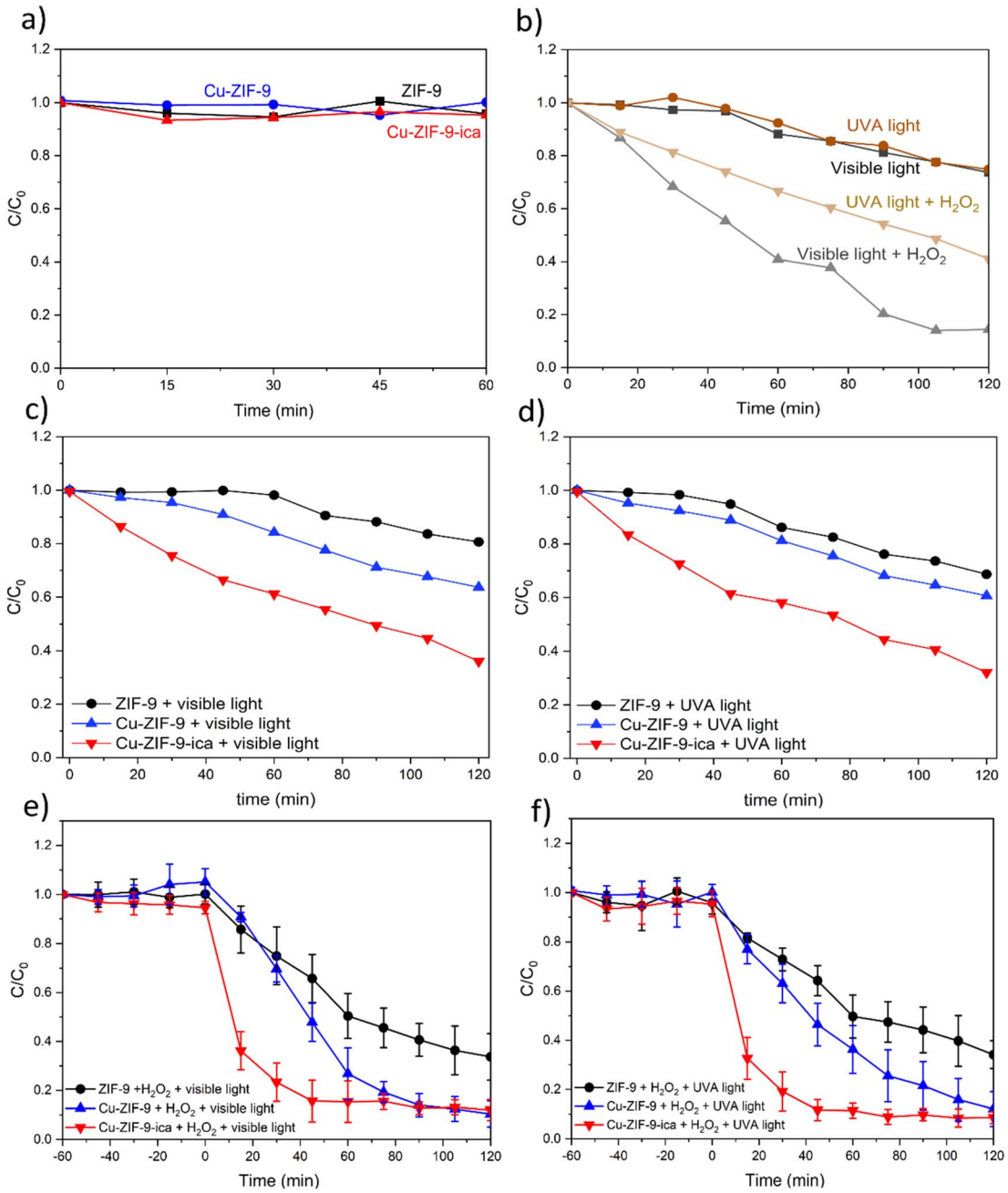

Fig. 3 MB adsorption process with ZIF-9 (■), Cu-ZIF-9 (●) and Cu-ZIF-9-ica (▲) (a). MB degradation by photolysis with visible (■) and UVA (●) light alone and combined action of H_2O_2 and visible (▲) or UVA (▼) light (b). Photocatalysis process without H_2O_2 under visible light: ZIF-9 (●), Cu-ZIF-9 (▲) and Cu-ZIF-9-ica (▼) (c) and UVA light: ZIF-9 (●), Cu-ZIF-9 (▲) and Cu-ZIF-9-ica (▼) (d). Photo-Fenton process with H_2O_2 (10 mM) under visible light: ZIF-9 (●), Cu-ZIF-9 (▲) and Cu-ZIF-9-ica (▼) (e), and UVA light: ZIF-9 (●), Cu-ZIF-9 (▲) and Cu-ZIF-9-ica (▼) (f).

molecules.[36] These results are in agreement with those observed by Peter *et al.*, who reported removal of MB (27%) in a UV reactor with a 150 W Hg lamp,[3] and with those of Zhang *et al.*,[37] who used a 350 W xenon lamp with a 420 nm UV-cutoff filter. We must note that in our experiments the power of the visible light source was 1.7 times higher than that of the UV-light source. In this context, evaluation of the combined action of H_2O_2 and light revealed a greater degradation of the contaminant, reaching 80% degradation under visible light after 105 min and 60% degradation under UV light at the end of the test. The results of this study can be explained by the difference in power between the lamps. The degradation results under the combined H_2O_2/light action can be attributed to the good production of $^{\bullet}OH$ radicals due to the electron accepting nature of H_2O_2, which reacts with the electrons of the conduction band producing these radicals.[38] Additional experiments were conducted to evaluate the photocatalytic activity of the materials under visible light and UV light without H_2O_2 (included in Fig. 3c and d). These results clearly demonstrate that, in the absence of H_2O_2, the photocatalytic activity of the materials is significantly reduced. This effect is particularly evident for ZIF-9 and Cu-ZIF-9, both of which show minimal pollutant degradation under these conditions. However, Cu-ZIF-9-ica exhibits a more noticeable degradation, which is attributed to enhanced light absorption and possibly improved charge transfer facilitated by the presence of Cu and the ica ligand.

The degradation process improves very significantly when catalysts are added (Fig. 3e and f) compared to the tests with only hydrogen peroxide and light (Fig. 3b). MB degradation reached 92% through heterogeneous photo-Fenton using Cu-ZIF-9-ica (UPO-3) under visible light (Fig. 3e) and 90% under UVA light in only 45 min (Fig. 3f). These values are much higher than those achieved with Cu-ZIF-9 (54 and 53% under visible and UVA light) or ZIF-9 (34 and 32% under visible and UVA light) at 45 min, respectively. Reproducibility, with an error margin of 6%, is also acceptable, as its manipulation is complicated due to the hydrophilic nature of ZIF-9 (Fig. 3e and f). Since the combined action of H_2O_2 and light produced a degradation rate that is almost equal to that of ZIF-9 samples under visible and UVA light, it is inferred that bare ZIF-9 has a very low photocatalytic activity. It is noteworthy that the rate of degradation increased by approximately 50% in the first 15 minutes with Cu-ZIF-9-ica as compared to Cu-ZIF-9. This behaviour experimentally demonstrates the important influence of multivariate the composition by the simultaneous presence of Cu^{2+} and a band modulating ligand into the MOF. This is expected to increase light absorption and electron excitation to produce a larger number of $^{\bullet}OH$ radicals and prevent the rapid recombination of electron holes.[17]

It should be noted that the degradation efficiency of MB by heterogeneous photo-Fenton using UPO-3 (Cu-ZIF-9-ica) is higher than the efficacy of traditional Fenton catalysts such as iron oxides. For example, the degradation of 98% of MB in the Fe_2O_3-kaolin/H_2O_2/vis system reached 98% in 120 min (6 times longer) even with a 5 times higher concentration of H_2O_2 and a much higher lamp power than that used in our study.[39] Other Au–Fe_3O_4/graphene catalysts do not achieve degradation under visible light even in 120 min and have to use UV to achieve complete degradation in that time.[40] To obtain comparable results, iron oxide, in this case in a ternary nanocomposite (TiO_2-rGO-Fe_2O_3), also required using again 5 times more H_2O_2 than our work and a more powerful visible lamp of 150 watts.[41] Moreover, the degradation efficiency of MB by heterogeneous photo-Fenton using UPO-3 (Cu-ZIF-9-ica) is higher than the average results reported in the literature with other modified MOFs. There are many studies that achieved less degradation in more time and under more vigorous conditions.[5,42,43] Yu *et al.*[44] demonstrated a significant degradation of MB (93%) using ZnO@ZIF-8 nanospheres. They used a higher concentration of H_2O_2 (0.5 M) compared to the concentration used in this study (10 mM), over a longer duration (150 min) and under a 500 W visible light xenon lamp. Somnath *et al.* synthesized {[Co_3(-BTC)$_2$(Bimb)$_{2.5}$]·2H_2O}n to degrade 94.1% of MB in 240 min by adding the same concentration of H_2O_2 as in this study, but using a higher power mercury UV lamp (300 W).[45] In another study, a cobalt MOF with a mixed ligand was used, reaching only 47.4% MB degradation in 135 min under UV irradiation with a rate constant much lower than that in this study.[46] It can be concluded that the synthesized materials reach a high percentage of elimination in a short time under mild conditions in the photocatalytic reaction concerning determining parameters such as the concentration of H_2O_2 or radiation intensity.

All heterogeneous photo-Fenton reactions studied here follow first-order kinetics (eqn (1) and Fig. S.6†), as typically occurs in these processes.[47–50] Under visible light, the reaction using Cu-ZIF-9 is twice as fast (k = 0.0176 min^{-1}) as that using pure ZIF-9 (0.0081 min^{-1}). The reaction rate triples when the MOF is doped with Cu^{2+} (0.0282 min^{-1}) and is exposed to UVA light. This confirms the positive influence of the incorporation of Cu^{2+} on the increase in active metal centres for the production of $^{\bullet}OH$ radicals.[47] Likewise, the presence of the metal prevents the rapid recombination of electron holes, thus improving the photocatalytic activity of the material.[17] According to Grau-Crespo *et al.*, incorporating a transition metal (Cu) in the tetrahedral position of mixed-bond ZIFs can enhance photon absorption and simultaneously extend the recombination times of electrons and holes.[17] This is due to the overlap between the empty metal levels and the less occupied crystal orbitals of the structure. As reported in the literature, the absorption of light by the MOF with Cu leads to the generation of e^-/h^+ pairs on the surface of the photocatalyst and the electrons are trapped by Cu^+/Cu^{2+}.[51] The Cu^+ form of copper acts efficiently as an electron scavenger and helps restrict the recombination of e^- and h^+. These electrons combined with oxygen molecules dissolved in water and holes in the valence band are captured by H_2O_2 species on the surface of the catalyst to form hydroxyl radicals, following the reactions below (eqn (2)–(8)):[52]

$$\text{MOF} + Cu^{2+}/Cu^{+} + \text{radiation}(h\nu) \rightarrow \text{MOF}(h^+) + Cu^{2+}/Cu^{+}(e^-) \quad (2)$$

$$H_2O_2 + e^- \rightarrow {}^{\bullet}OH + OH^- \quad (3)$$

$$Cu^{2+} + H_2O_2 \rightarrow Cu^{+} + {}^{\bullet}OOH + H^+ \quad (4)$$

$$Cu^{+} + H_2O_2 \rightarrow Cu^{2+} + {}^{\bullet}OH + OH^{-} \quad (5)$$

$$h^{+} + {}^{\bullet}OH + MB \rightarrow \text{degraded products} \quad (6)$$

$$Cu^{+} + H_2O_2 + H^{+} \rightarrow Cu^{2+} + H_2O + {}^{\bullet}OH \quad (7)$$

$$MB + {}^{\bullet}OH \rightarrow \text{degraded compounds} \quad (8)$$

Moreover, it has been possible to increase the kinetics of Cu-ZIF-9-ica more than five times with respect to ZIF-9 by adding the metal and the ligand, with a kinetic constant of 0.0467 min^{-1} under visible light and 0.0475 min^{-1} under UVA light compared to 0.0081 min^{-1} under visible light and 0.0088 min^{-1} under UVA light for ZIF-9. This can be attributed to the decrease in the band gap due to the addition of copper and the presence of the ligand, with the corresponding increase of light absorption and thus electron excitation. Previous studies reported a band gap of 4.6 eV for $Zn(bIm)_2$ and 3.8 eV for Zn(ica),[17] which is consistent with the results obtained here from first-principles calculations and experimental band gaps obtained by DRS (Fig. S7†). The computed electronic band gaps range from 4.51 to 4.11 eV for ZIF-9, from 4.54 to 3.32 eV for Cu-ZIF-9, and from 3.03 to 2.76 eV for Cu-ZIF-9-ica, in comparison with the experimental band gaps of 3.81 eV, 2.90 eV and 2.70 eV for ZIF-9, Cu-ZIF-9 and Cu-ZIF-9-ica, respectively. These differences likely arise from experimental effects such as defect states or band broadening. These values indicate that ZIF-9 and Cu-ZIF-9 are primarily photoactivated under UV light, as their band gaps exceed the visible light absorption threshold (<3.1 eV). This is supported by the experimental results (Fig. 3e and f), where both materials showed negligible MB degradation under visible light in comparison with the control experiment (H_2O_2 + visible light) (Fig. 3b). However, Cu-ZIF-9 exhibited enhanced MB degradation under UV light (≈20%), suggesting direct photoactivation and increased reactive oxygen species (ROS) generation. In contrast, UPO-3 (Cu-ZIF-9-ica), with a smaller band gap, demonstrated significant activity under visible light, highlighting its greater potential for visible-light-driven photocatalysis.

We have rationalized that the incorporation of the ica ligand generates electron acceptor sites,[53] which can increase the positive charges on the surface of the semiconductor, partially consuming electrons, and thus reducing the probability of the combination of holes, h^{+}, with e^{-}. Additionally, the increase in the surface area of Cu-ZIF-9-ica might facilitate the exposure of active sites and the interaction between the MOF and the reactant species.[54] Shen *et al.* determined that the introduction of functional groups into the organic structure of UiO-66 affects the electron density of the metal centre.[55] The higher electron density caused by this electron-donating functional group promotes the separation and transfer of photogenerated charge carriers. As a result, the photocatalytic activity of the material was improved. Jin *et al.* corroborated this statement in their study in which they synthesized three MOFs: UiO-66-NO_2, UiO-66-NH_2 and UiO-66-NO_2/UiO-66-NH_2, of which the only one that showed greater photocatalytic activity was that containing a mixture of a metal and ligand added to its structure.[13] As noted above, engineering ZIF-9 improves the photocatalytic properties, which can be understood on an atomistic background. First, it is worth noting that the overall structural properties do not change significantly at the unit cell level (Fig. 4), due to the flexibility of the ZIF-9 framework that can accommodate the local distortions. The tetrahedral angles and tetrahedricity are important structural features in zeolite topology materials,[56] and an analysis of the distortions of the tetrahedra can shed light on the effects of the modifications.

When comparing the tetrahedral N–metal–N angles around the Cu atoms in Cu-ZIF-9 with those in ZIF-9, the sum of the difference per Cu atom is 40.0°. This value decreases by 20% to 32.8 when the ica ligands are included (Cu-ZIF-9-ica). The

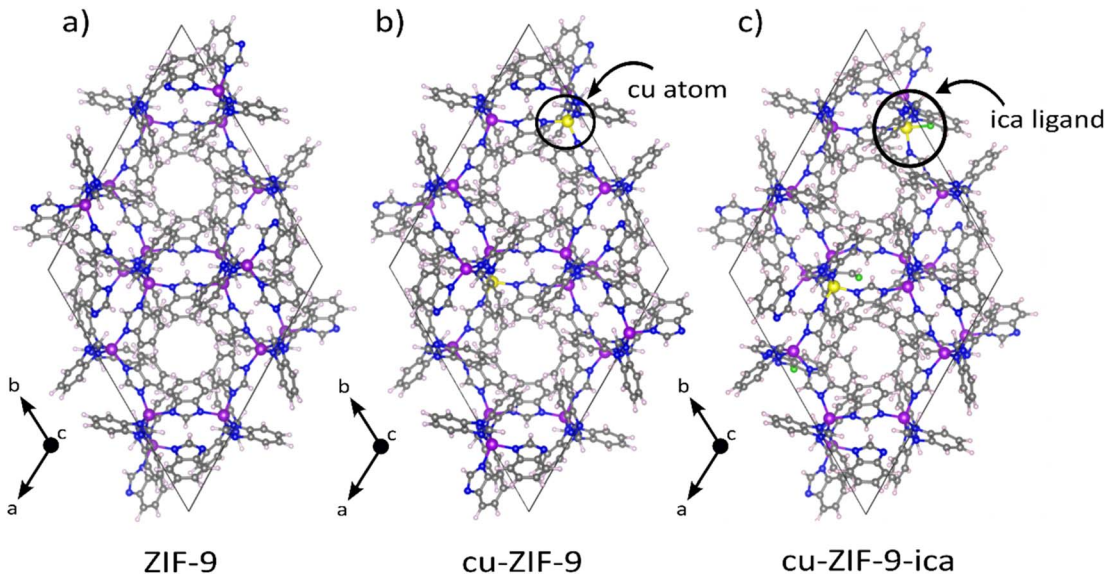

Fig. 4 DFT optimised structures of ZIF-9 (a), Cu-ZIF-9 (b) and Cu-ZIF-9-ica (c). Colour code: yellow – Cu atoms, purple – Co atoms, blue – N atoms, grey – C atoms, white – H atoms, and green – O atoms.

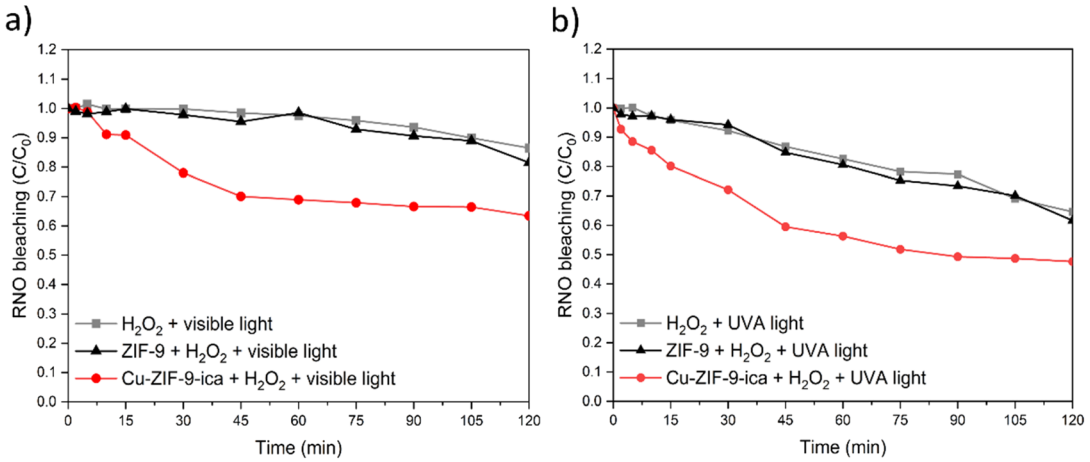

Fig. 5 RNO bleaching by H_2O_2 + light (■), ZIF-9 + H_2O_2 + light (▲) and Cu-ZIF-9-ica + H_2O_2 + light (●) under visible light (a) and UVA (b).

favoured structural features of Cu-ZIF-9-ica over ZIF-9-ica can explain the larger Cu incorporation observed in Cu-ZIF-9-ica. The calculated REPEAT atomic charges also provide valuable information on the role of Cu atoms and ica ligands. In ZIF-9 cobalt charges are in the range of 1.00 and 1.02*e*. Upon incorporation of Cu, they remain in the same range, but the atomic charges of the Cu atoms are much lower, *i.e.* 0.61*e*. A further decrease in Cu charges to 0.48 and 0.56*e* occurs when ica ligands are added to the framework. The macroscopic result is expected to be a decrease in electron–hole recombination, as mentioned above. The production of ˙OH radicals was confirmed using *p*-nitrosodimethylaniline (RNO), a probe compound that acts as a spin trap for the detection of these radicals. Bleaching of RNO has been reported to be very selective to oxidation of ˙OH radicals, as it does not react with singlet oxygen, superoxide anions, or other peroxy compounds.[57] Cu-ZIF-9-ica showed improved degradation of RNO compared to ZIF-9 and its control experiment without catalysts (Fig. 5). The

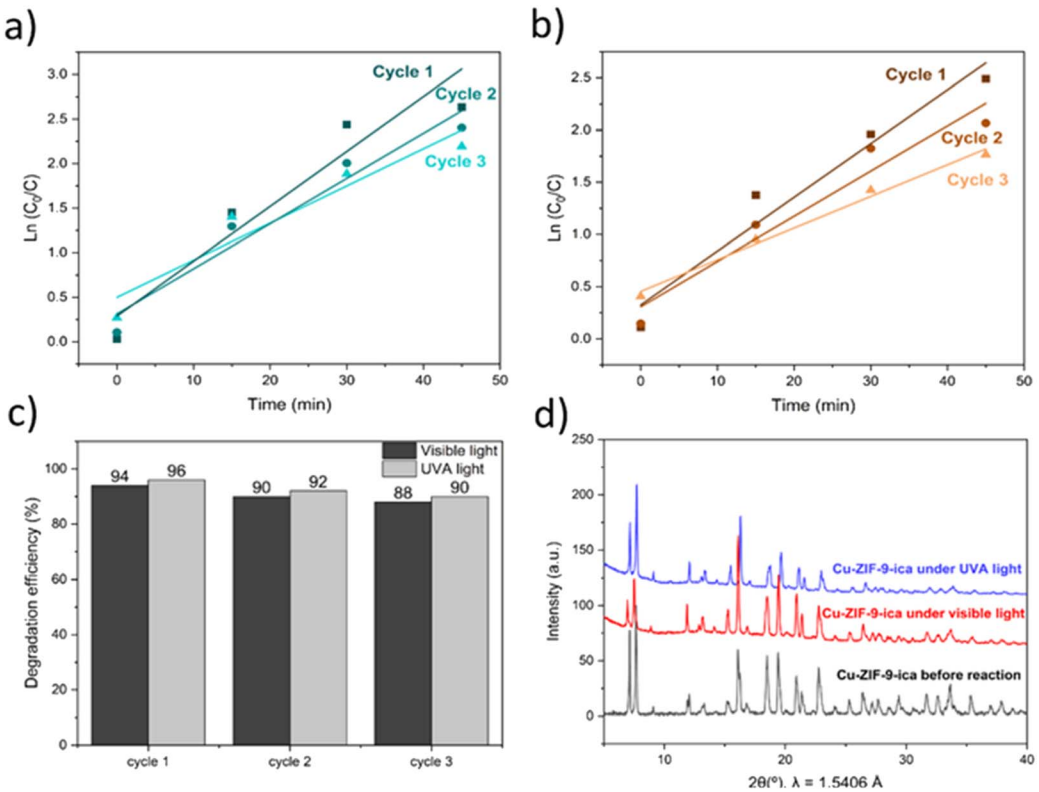

Fig. 6 First order kinetics over 3 cycles of reusability of Cu-ZIF-9-ica under visible light (a) and UVA light (b). Degradation efficiency for Cu-ZIF-9-ica under visible and UVA light in 3 cycles (c), and XRD analysis of Cu-ZIF-9-ica before and after 3 cycles (d).

results show that ZIF-9 produces negligible hydroxyl radicals under the tested conditions, consistent with its minimal photocatalytic activity observed under visible light and UVA irradiation (Fig. 3e and f). This suggests that the limited ROS generation in the presence of ZIF-9 results from the direct photolysis of H_2O_2, independent of any catalytic contribution. In contrast, UPO-3 (Cu-ZIF-9-ica) exhibits significantly higher activity, in both pollutant degradation and RNO bleaching (Fig. 5a and b; red line), confirming the enhanced production of hydroxyl radicals. This indicates that Cu/ica incorporation acts as a sink for conduction band electrons, reducing the rate of charge carrier recombination and leading to increased hydroxyl radical production.[24]

The reusability of the MOF is crucial in the search for green solutions for applying photocatalytic processes in heterogeneous systems.[58] Therefore, to evaluate the stability of the UPO-3 catalyst, Cu-ZIF-9-ica, three recycling cycles were carried out under UVA and visible light. High levels of reuse were obtained without relevant loss in reaction kinetics, with rates of 0.0587 min^{-1}, 0.0451 min^{-1} and 0.0311 min^{-1} for cycles 1, 2 and 3 respectively under visible light and 0.04066 min^{-1}, 0.0428 min^{-1} and 0.0321 min^{-1} for cycles 1 to 3, respectively, under UVA light (Fig. 6a and b). This indicated only a 6% loss of efficiency after three cycles (Fig. 6c), which could be attributed to irreversible adsorption of contaminant molecules in the active sites of the catalyst.[5,59,60] It is important to note that the structure of the MOF is maintained after the photocatalytic treatments. The XRD results of Cu-ZIF-9-ica after 3 cycles under visible and UVA light showed good stability under water (Fig. 6d). Furthermore, the leaching of Co^{2+} and Cu^{2+} after the photocatalysis test under visible and UVA light was quantified *via* MS-ICP analysis. It was found that Cu-ZIF-9-ica samples leached 0.002% of Co^{2+}, while leaching of Cu^{2+} was not detected. These results confirm that, with no significant leaching, Cu-ZIF-9-ica maintains its structure and remains reusable for at least three cycles without a relevant loss of efficiency.

Conclusions

This research designs multivariate ZIF-9 with copper and ica ligands to greatly improve its photocatalytic efficiency for heterogeneous photo-Fenton-like reactions. Highly crystalline ZIF-9, Cu-ZIF-9, and Cu-ZIF-9-ica were synthesized using a simpler and more environmentally friendly solvothermal method compared to the conventional one, which replaces the solvent DMF with ethanol. The successful doping of Cu^{2+} and the incorporation of the ligand 2-imidazolecarboxaldehyde, to form UPO-2, were confirmed through various characterization techniques. Moreover, it is worth noting that the difficulty of incorporating Cu in ZIF-9 is solved with the addition of the ica ligand. UPO-3, Cu-ZIF-9-ica, demonstrates a significant improvement in the photocatalytic properties of the MOF, achieving a 95% degradation of MB within only 45 min under low hydrogen peroxide concentration, neutral pH, and exposure to both visible and UVA light. The introduction of a mixed ligand results in a doubling of the degradation rate with Cu-ZIF-9-ica compared to the addition of the metal alone, Cu-ZIF-9, and a fivefold increase compared to ZIF-9, in agreement with calculated band gaps and changes in atomic charges. This highlights the critical role of the incorporation of metals together with mixed ligands in enhancing the photocatalytic properties of MOFs.

Furthermore, UPO-3 (Cu-ZIF-9-ica) exhibited robust chemical and structural stability for repeated MB degradation cycles and showed no metal leaching, indicating its environmental friendliness. This study demonstrates the great potential of Cu-ZIF-9-ica for practical applications, as it has been shown to be efficient at low concentration, room temperature and neutral pH under visible light and therefore sunlight could be used in experiments on a larger scale. Future research should focus on developing materials with stable catalytic performance, while improving their recoverability and reducing catalyst loss during the recovery process. In addition, these materials will need to be thoroughly tested in real-world water treatment scenarios, alongside the creation of new methodologies to ensure scalability, enabling their use in industrial applications.

Data availability

The data supporting this article have been included as part of the ESI.†

Author contributions

Menta Ballesteros and A. Rabdel Ruiz Salvador contributed to the study conception and design. Material preparation and data collection were performed by Noelia Rodríguez-Sánchez, Paula Prieto-Laria, Carsten Prinz and A. Rabdel Ruiz Salvador (DFT), while data analysis was performed by all authors. The first draft of the manuscript was written by Noelia Rodríguez-Sánchez and all authors contributed to the writing of the final version. All the authors read and approved the final version of the manuscript.

Conflicts of interest

There are no conflicts to declare.

Acknowledgements

We would like to thank Ines Feldmann for the SEM images. We also acknowledge funding for VALZEO project from the European Commission (HORIZON MSCA-2021-SE-01 under grant agreement no. 101086354). P. Prieto-Laria is a beneficiary of a research assistant contract from "Programa Investigo" (Next Generation EU). We are grateful to C3UPO for providing high performance computing facilities.

Notes and references

1 W. Musie and G. Gonfa, *Heliyon*, 2023, **9**, e18685.
2 N. Kalboussi, Y. Biard, L. Pradeleix, A. Rapaport, C. Sinfort and N. Ait-mouheb, *Sci. Total Environ.*, 2022, **836**, 155486.

3 A. Peter, A. Mihaly-Cozmuta, C. Nicula, L. Mihaly-Cozmuta, A. Jastrzębska, A. Olszyna and L. Baia, *Water, Air, Soil Pollut.*, 2017, **228**, 41.
4 M. Zhang, L. Wang, T. Zeng, Q. Shang, H. Zhou, Z. Pan and Q. Cheng, *Dalton Trans.*, 2018, **47**, 4251–4258.
5 I. Y. Habib, J. Burhan, F. Jaladi, C. M. Lim, A. Usman, N. T. R. N. Kumara, S. C. E. Tsang and A. H. Mahadi, *Catal. Today*, 2021, **375**, 506–513.
6 Q. Guo, C. Yan, Z. Huang, Y. Liu, D. Cheng, C. Lu, J. Ran and Y. Yang, *Nanoscale*, 2024, **16**, 12957–12966.
7 Y. Deng and R. Zhao, *Curr. Pollut. Rep.*, 2015, **1**, 167–176.
8 W. L. Duan, Y.-X. Li, Feng-Yan, W.-Z. Li and J. Luan, *J. Colloid Interface Sci.*, 2023, **646**, 107–117.
9 C. Gropp, S. Canossa, S. Wuttke, F. Gándara, Q. Li, L. Gagliardi and O. M. Yaghi, *ACS Cent. Sci.*, 2020, **6**, 1255–1273.
10 J. John, K. Ramesh and P. Velayudhaperumal Chellam, in *Advanced Materials for Sustainable Environmental Remediation*, Elsevier, 2022, pp. 155–174.
11 Y. Li, X. Li and B. Wang, *ACS Appl. Nano Mater.*, 2022, **5**, 2510–2521.
12 L. Zhu, F. Hu, B. Sun, S. Gu, T. Gao and G. Zhou, *Adv. Sustainable Syst.*, 2023, **7**, 2200394.
13 J.-C. Jin, M. Yang, Y.-L. Zhang, A. Dutta, C.-G. Xie and A. Kumar, *J. Taiwan Inst. Chem. Eng.*, 2021, **129**, 410–417.
14 C. Shan, X. Zhang, S. Ma, X. Xia, Y. Shi and J. Yang, *Colloids Surf., A*, 2022, **636**, 128108.
15 K. S. Park, Z. Ni, A. P. Côté, J. Y. Choi, R. Huang, F. J. Uribe-Romo, H. K. Chae, M. O'Keeffe and O. M. Yaghi, *Proc. Natl. Acad. Sci. U.S.A.*, 2006, **103**, 10186–10191.
16 L. Chen, Y. Peng, H. Wang, Z. Gu and C. Duan, *Chem. Commun.*, 2014, **50**, 8651.
17 R. Grau-Crespo, A. Aziz, A. W. Collins, R. Crespo-Otero, N. C. Hernández, L. M. Rodriguez-Albelo, A. R. Ruiz-Salvador, S. Calero and S. Hamad, *Angew. Chem., Int. Ed.*, 2016, **55**, 16012–16016.
18 M. He, J. Yao, Q. Liu, Z. Zhong and H. Wang, *Dalton Trans.*, 2013, **42**, 16608.
19 T. D. Kühne, M. Iannuzzi, M. Del Ben, V. V. Rybkin, P. Seewald, F. Stein, T. Laino, R. Z. Khaliullin, O. Schütt, F. Schiffmann, D. Golze, J. Wilhelm, S. Chulkov, M. H. Bani-Hashemian, V. Weber, U. Borštnik, M. Taillefumier, A. S. Jakobovits, A. Lazzaro, H. Pabst, T. Müller, R. Schade, M. Guidon, S. Andermatt, N. Holmberg, G. K. Schenter, A. Hehn, A. Bussy, F. Belleflamme, G. Tabacchi, A. Glöß, M. Lass, I. Bethune, C. J. Mundy, C. Plessl, M. Watkins, J. VandeVondele, M. Krack and J. Hutter, *J. Chem. Phys.*, 2020, **152**, 194103.
20 J. Heyd, G. E. Scuseria and M. Ernzerhof, *J. Chem. Phys.*, 2003, **118**, 8207–8215.
21 K. L. Svane, J. K. Bristow, J. D. Gale and A. Walsh, *J. Mater. Chem. A*, 2018, **6**, 8507–8513.
22 C. Campañá, B. Mussard and T. K. Woo, *J. Chem. Theory Comput.*, 2009, **5**, 2866–2878.
23 S. Hamad, S. R. G. Balestra, R. Bueno-Perez, S. Calero and A. R. Ruiz-Salvador, *J. Solid State Chem.*, 2015, **223**, 144–151.
24 B. R. Cruz-Ortiz, J. W. J. Hamilton, C. Pablos, L. Díaz-Jiménez, D. A. Cortés-Hernández, P. K. Sharma, M. Castro-Alférez, P. Fernández-Ibañez, P. S. M. Dunlop and J. A. Byrne, *Chem. Eng. J.*, 2017, **316**, 179–186.
25 K. V. Kumar, K. Porkodi and F. Rocha, *Catal. Commun.*, 2008, **9**, 82–84.
26 Z. Öztürk, J. P. Hofmann, M. Lutz, M. Mazaj, N. Z. Logar and B. M. Weckhuysen, *Eur. J. Inorg. Chem.*, 2015, **2015**, 1625–1630.
27 L. T. L. Nguyen, K. K. A. Le, H. X. Truong and N. T. S. Phan, *Catal. Sci. Technol.*, 2012, **2**, 521–528.
28 S. Das and V. C. Srivastava, *Mater. Sci. Semicond. Process.*, 2017, **57**, 173–177.
29 Y. Zhao, Z. Sun, S. Liu, Z. Li, X. Mao, S. Wang and R. Hao, *AIP Adv.*, 2022, **12**, 025113.
30 G. Khandelwal, N. P. Maria Joseph Raj and S. Kim, *Adv. Funct. Mater.*, 2020, **30**, 1910162.
31 Y. Ban, Y. Li, X. Liu, Y. Peng and W. Yang, *Microporous Mesoporous Mater.*, 2013, **173**, 29–36.
32 H. T. Kwon, H.-K. Jeong, A. S. Lee, H. S. An, T. Lee, E. Jang, J. S. Lee and J. Choi, *Chem. Commun.*, 2016, **52**, 11669–11672.
33 W. Chaikittisilp, N. L. Torad, C. Li, M. Imura, N. Suzuki, S. Ishihara, K. Ariga and Y. Yamauchi, *Chem.–Eur. J.*, 2014, **20**, 4217–4221.
34 A. Ebrahimi and M. Mansournia, *J. Phys. Chem. Solids*, 2017, **111**, 12–17.
35 M. Ebrahimi and M. Mansournia, *Mater. Lett.*, 2017, **189**, 243–247.
36 I. Groeneveld, M. Kanelli, F. Ariese and M. R. Van Bommel, *Dyes Pigm.*, 2023, **210**, 110999.
37 Y. Zhang, J. Zhou, Q. Feng, X. Chen and Z. Hu, *Chemosphere*, 2018, **212**, 523–532.
38 S. S. Shinde, C. H. Bhosale and K. Y. Rajpure, *Catal. Rev.*, 2013, **55**, 79–133.
39 S. Guo, G. Zhang and J. Wang, *J. Colloid Interface Sci.*, 2014, **433**, 1–8.
40 R. Saleh and A. Taufik, *Environ. Nanotechnol., Monit. Manage.*, 2019, **11**, 100221.
41 S. Banerjee, P. Benjwal, M. Singh and K. K. Kar, *Appl. Surf. Sci.*, 2018, **439**, 560–568.
42 S. Metin and D. İ. Çifçi, *J. Chem. Technol. Biotechnol.*, 2023, **98**, 1158–1165.
43 G. Maniakova, K. Kowalska, S. Murgolo, G. Mascolo, G. Libralato, G. Lofrano, O. Sacco, M. Guida and L. Rizzo, *Sep. Purif. Technol.*, 2020, **236**, 116249.
44 B. Yu, F. Wang, W. Dong, J. Hou, P. Lu and J. Gong, *Mater. Lett.*, 2015, **156**, 50–53.
45 M. A. Somnath and K. A. Siddiqui, *J. Mol. Struct.*, 2022, **1265**, 133399.
46 K. T. Alamgir, Y.-J. Wang, R. Ullah, B. Wang, L. Wang, W. Wu, S. Chen, L.-H. Xie and J.-R. Li, *RSC Adv.*, 2021, **11**, 23838–23845.
47 T. T. Minh, N. T. T. Tu, T. T. Van Thi, L. T. Hoa, H. T. Long, N. H. Phong, T. L. M. Pham and D. Q. Khieu, *J. Nanomater.*, 2019, **2019**, 1–16.
48 X. Xue, Y. Weng, S. Yang, S. Meng, Z. Zhang, G. Yi and Y. Zhang, *Environ. Sci. Pollut. Res.*, 2021, **28**, 15883–15889.

49 J.-C. Jin, M. Ray, B. Wu, Z.-J. Zhou, X. Wang, M. Muddassir and A. Mohanty, *J. Solid State Chem.*, 2023, **327**, 124283.
50 A. Modwi, M. A. Ghanem, A. M. Al-Mayouf and A. Houas, *J. Mol. Struct.*, 2018, **1173**, 1–6.
51 S. Y. Hao, S. X. Hou, J. Zhu and G. Hua Cui, *Polyhedron*, 2017, **134**, 88–98.
52 M. Zhu, Y. Liu, M. Chen, M. Sadrzadeh, Z. Xu, D. Gan, Z. Huang, L. Ma, B. Yang and Y. Zhou, *J. Membr. Sci.*, 2021, **640**, 119755.
53 L. Jiang, W. Zhang, C. Luo, D. Cheng and J. Zhu, *Ind. Eng. Chem. Res.*, 2016, **55**, 6365–6372.
54 B. Liu, X. Chen, N. Huang, S. Liu, Y. Wang, X. Lan, F. Wei and T. Wang, *Nat. Commun.*, 2023, **14**, 4835.
55 L. Shen, R. Liang, M. Luo, F. Jing and L. Wu, *Phys. Chem. Chem. Phys.*, 2015, **17**, 117–121.
56 S. R. G. Balestra, N. Rodríguez-Sánchez, D. Mena-Torres and A. R. Ruiz-Salvador, *Cryst. Growth Des.*, 2024, **24**, 938–946.
57 M. E. Simonsen, J. Muff, L. R. Bennedsen, K. P. Kowalski and E. G. Søgaard, *J. Photochem. Photobiol., A*, 2010, **216**, 244–249.
58 M. Cheng, C. Lai, Y. Liu, G. Zeng, D. Huang, C. Zhang, L. Qin, L. Hu, C. Zhou and W. Xiong, *Coord. Chem. Rev.*, 2018, **368**, 80–92.
59 P. Hayati, Z. Mehrabadi, M. Karimi, J. Janczak, K. Mohammadi, G. Mahmoudi, F. Dadi, M. J. S. Fard, A. Hasanzadeh and S. Rostamnia, *New J. Chem.*, 2021, **45**, 3408–3417.
60 X.-H. Sun, S.-H. Chen, Q.-Z. Guo, Z.-C. Shen, J. Wu and Z.-X. Du, *Sep. Purif. Technol.*, 2023, **324**, 124506.